Electrical Power and Energy Systems 69 (2015) 327–334

Contents lists available at ScienceDirect

Electrical Power and Energy Systems

journal homepage: www.elsevier.com/locate/ijepes

An active power control strategy for a DFIG-based wind farm to depress the subsynchronous resonance of a power system

Bin Zhao [a,b], Hui Li [a,*], Mingyu Wang [a], Yaojun Chen [a], Shengquan Liu [a], Dong Yang [a], Chao Yang [a], Yaogang Hu [a], Zhe Chen [c], Senior Member, IEEE

[a] State Key Laboratory of Power Transmission Equipment and System Security and New Technology (Chongqing University), Shapingba District, Chongqing 400044, China
[b] Sichuan Electric Vocational and Technical College, Chengdu 610072, China
[c] Institute of Energy Technology, Aalborg University, Aalborg East DK-9220, Denmark

ARTICLE INFO

Article history:
Received 30 January 2014
Received in revised form 3 January 2015
Accepted 3 January 2015

Keywords:
Doubly fed induction generator
Wind farms
Subsynchronous resonance
Auxiliary damping control
Parameter optimization

ABSTRACT

This study presents a novel auxiliary damping control strategy to depress subsynchronous resonance (SSR) oscillations in nearby turbine generators. In the proposed control strategy, SSR damping is achieved by adding turbine generator speed as a supplementary signal at the active power loop of the rotor-side converter (RSC) of doubly-fed induction generator (DFIG)-based wind farms. To design the SSR auxiliary damping controller, a transfer function between turbine generator speed and the output active power of the wind farms was introduced to derive the analytical expression of the damping coefficient. Then the damping effect of the active power of the DFIG-based wind farms was analyzed, and the phase range to obtain positive damping was determined. Next, the PID phase compensation parameters of the auxiliary damping controller were optimized by genetic algorithm to obtain the optimum damping in the entire subsynchronous frequency band. The last, the validity and effectiveness of the proposed auxiliary damping control were demonstrated on a modified version of the IEEE first benchmark model by time domain simulation analysis with the use of DigSILENT/PowerFactory.

Introduction

Series capacitive compensation is an important approach to improve the transfer capability and transient stability of existing transmission systems. However, the extensive use of series compensation can cause SSR, in which electrical networks exchange energy with the generator shaft system at frequencies less than the nominal frequency of the transmission line; this phenomenon results in turbine-generator shaft failure and instability of the power system [1,2].

To prevent the turbine-generator shaft from failing and to depress SSR oscillations, flexible AC transmission system (FACTS) devices (e.g., SVC, TCSC, STATCOM) [3–12], are widely utilized to effectively relieve SSR. These devices should be enhanced with an auxiliary damping controller to provide the extra damping characteristic. Although, the FACTS devices can depress SSR, but installation of such device is expensive, so utilizing FACTS may not be cost effective.

Wind energy is the fastest-growing form of renewable energy in the world because it is clean, non-polluting, and abundant. Wind farms with a scale of hundreds of MW level are increasingly being developed and connected to power systems. Doubly fed induction generators (DFIGs) are widely used in wind power plants because of their capability to decouple control of real and reactive power. With the integration of large-scale wind farms into power systems, some researchers have used the control capability of DFIG to damp power system oscillations; however, most studies have focused on damping inter-area low-frequency oscillations [13–16], whereas relatively very few studies have reported on damping SSR. Ref. [17] proposed the auxiliary control of a DFIG-based wind farm to damp SSR oscillations in nearby turbine generators by addition of a supplemental signal at the grid-side converter of the DFIG. However, the auxiliary controller requires the precise measurement of the angular speed deviation of each shaft segment. The controller parameters are obtained by a time-consuming trial-and-error approach, and the damping mechanism is also not analyzed. Therefore, the use of DFIG-based wind farms to damp SSR oscillations in the entire subsynchronous frequency band and the damping mechanism should be further analyzed.

This study presents the application of auxiliary damping control to the rotor-side converter (RSC) of a DFIG to damp SSR. A transfer function between turbine generator speed and the output active power of wind farms was introduced to derive the analytical

* Corresponding author. Tel.: +86 13883801036; fax: +86 23 65102441.
E-mail address: cqulh@163.com (L. Hui).

http://dx.doi.org/10.1016/j.ijepes.2015.01.002
0142-0615/

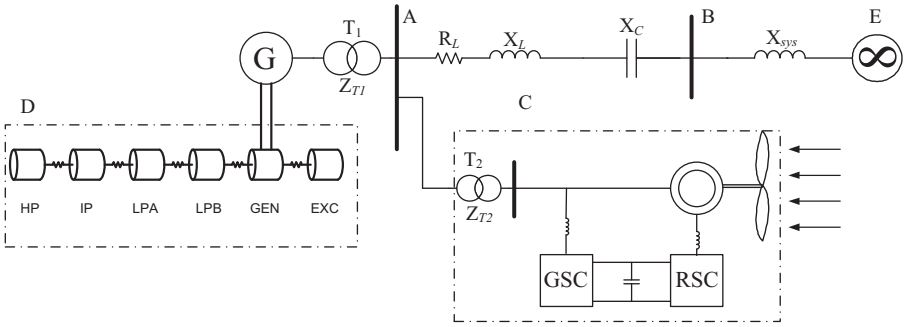

Fig. 1. Schematic of a DFIG-based wind farm connected to the IEEE first benchmark model.

expression of damping. The effect of the active power of the DFIG-based wind farms on system damping was analyzed, and the phase range to obtain positive damping was determined. Then, a new auxiliary damping control strategy was proposed. The PID phase compensation parameters of the auxiliary damping controller were optimized by genetic algorithm to obtain optimum damping in the entire subsynchronous frequency band. Finally, the IEEE first benchmark model, modified by the inclusion of the DFIG-based wind farms, is used to demonstrate the performance of the proposed auxiliary damping control to suppress SSR oscillations by time domain simulation analysis with the use of DigSILENT/PowerFactory.

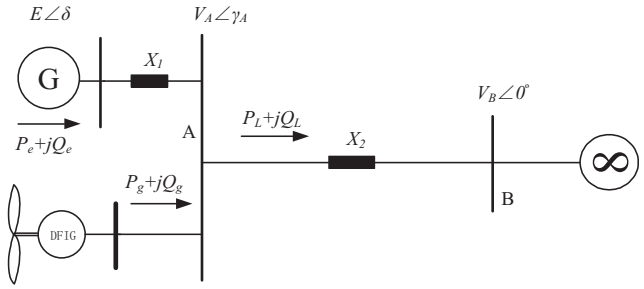

Fig. 3. Schematic of the simplified system model.

Power system model with DFIG based wind farm

To evaluate the effectiveness of the proposed strategy on auxiliary damping control, the well-known IEEE first benchmark model, modified by the inclusion of DFIG-based wind farms, is used (Fig. 1). The system consists of an 892.4 MWA turbine generator connected to an infinite bus through a radial series-compensated line. The rated voltage is 539 kV, and the frequency is 60 Hz. A DFIG-based wind farm (200 MW from the aggregation of 2 MW units) is connected to bus *A* via a transformer. Fig. 1 shows that G represents the turbine generators; C, the DFIG-based wind farms; D, the turbine shaft system; and E, the infinite power grid. $R_L + jX_L$ is the power transmission line impedance, X_c is the captance of the series compensation capacitor, and X_{sys} is the reactance of the transmission line to the infinite power grid. The complete electrical and mechanical data are given in Appendix.

Turbine generator shaft system model

The turbine generator shaft system consists of six shaft segments, namely, a high-pressure turbine (HP), an intermediate-pressure turbine (IP), a low-pressure turbine (LPA), a low-pressure

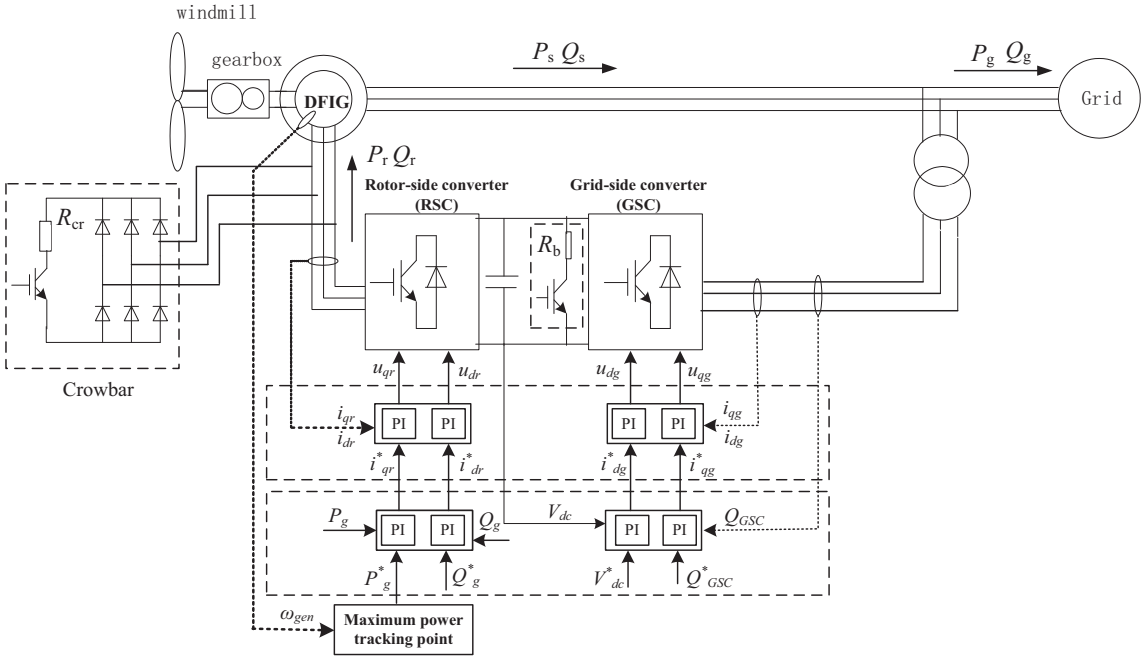

Fig. 2. Schematic of the DFIG wind turbine.

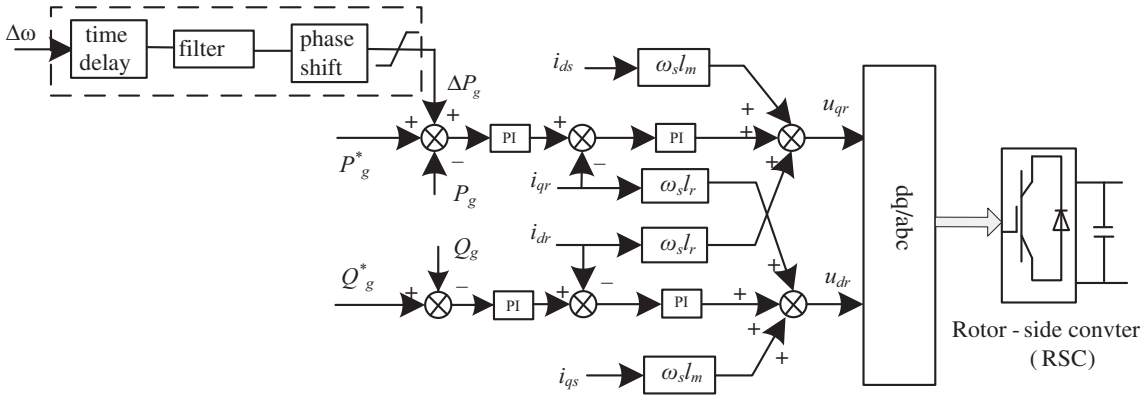

Fig. 4. Diagram of the auxiliary damping control system.

turbine (LPB), the generator (GEN), and the exciter (EXC). All masses are mechanically connected to one another by elastic shafts. The shaft system motion equation is described as follows:

where δ_i, ω_i, T_{Ji} are the angular displacement, angular velocity, and inertia time constant of the i-th mass of the shaft system, T_i is the dynamic torque that affects the i-th mass of the turbine generators,

$$\begin{cases} \Delta T_{HP} = 2T_{J1}\frac{d\Delta\omega_1}{dt} + D_{11}\Delta\omega_1 + D_{12}(\Delta\omega_1 - \Delta\omega_2) + k_{12}(\Delta\delta_1 - \Delta\delta_2) \\ \Delta T_{IP} = 2T_{J2}\frac{d\Delta\omega_2}{dt} + D_{22}\Delta\omega_2 + D_{12}(\Delta\omega_2 - \Delta\omega_1) + D_{23}(\Delta\omega_2 - \Delta\omega_3) + k_{12}(\Delta\delta_2 - \Delta\delta_1) + k_{23}(\Delta\delta_2 - \Delta\delta_3) \\ \Delta T_{LPA} = 2T_{J3}\frac{d\Delta\omega_3}{dt} + D_{33}\Delta\omega_3 + D_{23}(\Delta\omega_3 - \Delta\omega_2) + D_{34}(\Delta\omega_3 - \Delta\omega_4) + k_{23}(\Delta\delta_3 - \Delta\delta_2) + k_{34}(\Delta\delta_3 - \Delta\delta_4) \\ \Delta T_{LPB} = 2T_{J4}\frac{d\Delta\omega_4}{dt} + D_{44}\Delta\omega_4 + D_{34}(\Delta\omega_4 - \Delta\omega_3) + D_{45}(\Delta\omega_4 - \Delta\omega_5) + k_{34}(\Delta\delta_4 - \Delta\delta_3) + k_{45}(\Delta\delta_4 - \Delta\delta_5) \\ -\Delta T_e = 2T_{J5}\frac{d\omega_5}{dt} + D_{55}\Delta\omega_5 + D_{45}(\Delta\omega_5 - \Delta\omega_4) + D_{56}(\Delta\omega_5 - \Delta\omega_6) + k_{45}(\Delta\delta_5 - \Delta\delta_4) + k_{56}(\Delta\delta_5 - \Delta\delta_6) \end{cases} \quad (1)$$

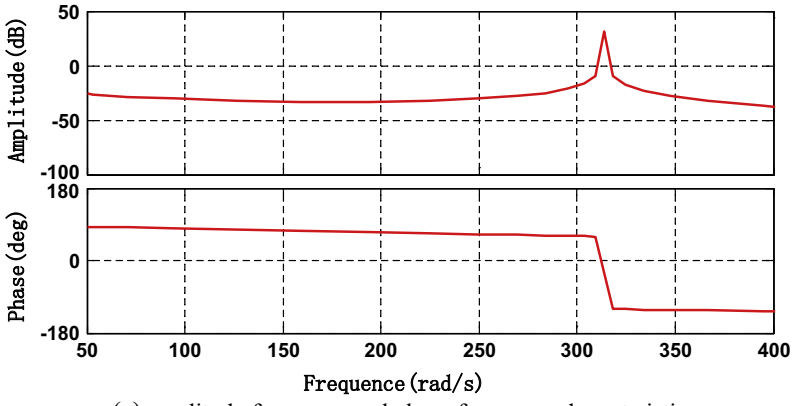

(a) amplitude-frequency and phase-frequency characteristic curve.

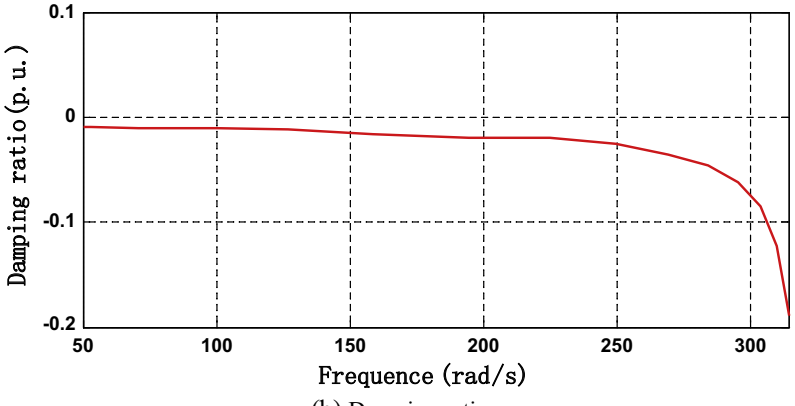

(b) Damping ratio curve

Fig. 5. Characteristics of the transfer function without auxiliary damping control.

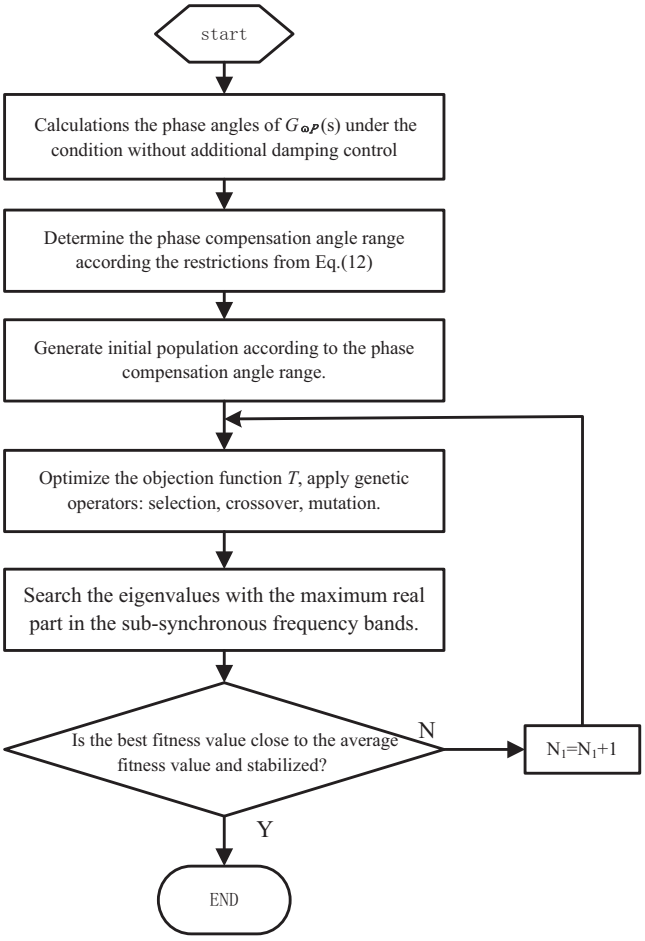

Fig. 6. Flowchart of the optimization of the PID controller parameters.

T_e is the electromagnetic torque of the turbine generator, and $k_{i,i+1}$ is the rigidity coefficient between the i-th and $i+1$-th masses. D_{ii} represents the self-damping ratio of the i-th mass, and $D_{i,i+1}$ is the mutual damping ratio between the i-th and $i+1$-th masses. The above equation can be simplified as follows:

$$\Delta \boldsymbol{T} = (\boldsymbol{T_J} p^2 + \boldsymbol{D} p + \boldsymbol{K})\Delta \boldsymbol{\delta} \tag{2}$$

where $\boldsymbol{T_J}$, $\boldsymbol{D}$ are the inertia time constant and the damping diagonal matrix, respectively, $\boldsymbol{K}$ is the rigidness coefficient tridiagonal matrix, and p is the differential operator.

DFIG-based wind turbine model

The typical DFIG configuration consists of a wound rotor induction generator, with the stator directly connected to the grid and the rotor interfaced through a back-to-back partial scale power converter, as shown in Fig. 2. The back-to-back converter is a bidirectional power converter that consists of two conventional voltage source converters (an RSC and a grid side converter or GSC) and a common dc-bus. Both GSC and RSC contain an internal current controller and an external power controller. The slow power controller provides a reference current to the fast current controller, which further regulates the rotor current to the reference value. The RSC aims to independently control the active power of the generator and the reactive power produced or absorbed from the grid. The GSC aims to keep the dc-link voltage constant regardless of the magnitude and direction of the rotor power and to guarantee converter operation with unity power factor (zero reactive power). This requirement means that the GSC exchanges only active power with the grid, so the transmission of reactive power from the DFIG to the grid is done only through the stator [17,18].

Analysis of SSR damping according to the active power of wind farms

To analyze the mechanism of influence of the DFIG-based wind farms on system SSR damping, the system model in Fig. 1 is simplified in Fig. 3, where E is the quadrature-axis transient electromotive force of turbine generator G; V_A is the voltage of bus A; V_B is the infinite bus voltage; δ, γ_A is the phase angle difference between E, V_A, and V_B; P_e, Q_e are the active/reactive power output of the turbine generator; P_g, Q_g are the active/reactive power output of the DFIG-based wind farms; P_L, Q_L are the active/reactive power flow through the transmission line; and X_1, X_2 are the reactance parameters.

The output active/reactive power P_e/Q_e of the turbine generator can be expressed as:

$$P_e = \frac{EV_A \sin(\delta - \gamma_A)}{X_1} \tag{3}$$

$$Q_e = \frac{EV_A}{X_1}\cos(\delta - \gamma_A) - \frac{V_A^2}{X_1} \tag{4}$$

Because of the active/reactive decoupling characteristics of power systems, the voltage microvariation caused by active power microvariation can be neglected. In other words, voltage V_A was considered as constant, and the linearization equation of Eq. (3) can be expressed as follows:

$$\Delta P_e = \frac{EV_A \cos(\theta_0)}{X_1}(\Delta\delta - \Delta\gamma_A) \tag{5}$$

where $\theta_0 = \delta_0 - \gamma_{A0}$. The subscript 0 represents an initial value.

Then, according to the active power balance of the transmission line, the next linearization equation can be obtained:

$$\frac{V_A V_B \cos(\gamma_{A0})}{X_2}\Delta\gamma_A = \Delta P_e + \Delta P_g \tag{6}$$

Eq. (5) was substituted into Eq. (6):

$$\Delta\gamma_A = k_0\Delta\delta + k_1\Delta P_g \tag{7}$$

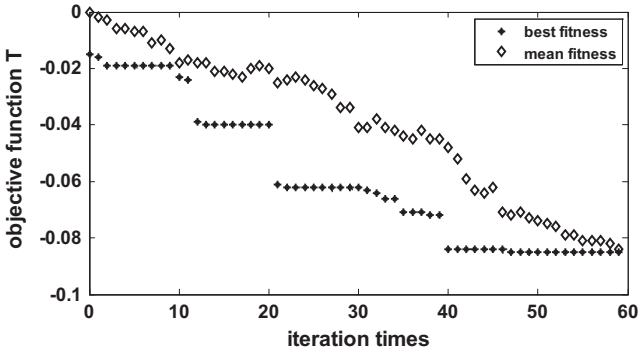

Fig. 7. Best fitness and mean fitness vs. iteration times.

Table 1
Optimization parameters of the PID controller.

	K_P	T_D/ms	T_I/ms
Active power loop	1	5.9	82

where $k_0 = \frac{X_2 E\cos(\theta_0)}{X_1 V_B \cos(\gamma_{A0}) + X_2 E\cos(\theta_0)}$, $k_1 = \frac{X_1 X_2}{X_1 V_A V_B \cos(\gamma_{A0}) + X_2 V_A E\cos(\theta_0)}$.

Next, Eq. (7) was substituted into Eq. (5), and ΔP_e can be rewritten as follows:

$$\Delta P_e = \frac{EV_A\cos(\theta_0)(1-k_0)}{X_1}\Delta\delta - \frac{EV_A k_1\cos(\theta_0)}{X_1}\Delta P_g \tag{8}$$

The above equation have two item, the first item is synchronous torque, the last item is related to DFIG active power ΔP_g, which may produce positive or negative damping effects on the system according to the phase relationship between ΔP_g and turbine generators $\Delta\omega$. To analyze the damping effects of active power ΔP_g on the system, this study introduced transfer function $G_{\omega P}(s)$ based on turbine generator speed $\omega(t)$ and the output active power $P_g(t)$ of the wind farms (referred to as the active-speed transfer function) as follows:

$$G_{\omega P}(s) = \frac{\Delta P_g(s)}{\Delta\omega(s)} \tag{9}$$

Given the sinusoidal microvariation of turbine generators $\Delta\omega$ with amplitude A and frequency ω_0 ($\Delta\omega = A\sin(\omega_0 t)$), the microvariation of active power ΔP_g can be expressed as follows:

$$\Delta P_g = A|G_{\omega P}(j\omega_0)|\sin(\omega_0 t + \angle G_{\omega P}(j\omega_0)) \tag{10}$$

To analyze the damping effects of the last item of Eq. (8), we define the component of the last item on $\Delta\omega$ as active power damping ratio $D_{\omega P}$:

$$D_{\omega P} = -\frac{EV_A k_1\cos(\theta_0)}{X_1}|G_{\omega P}(j\omega_0)|\cos(\angle G_{\omega P}(j\omega_0)) \tag{11}$$

When the phase angle between the range $\frac{\pi}{2} < \angle G_{\omega P}(j\omega_0) < \frac{3\pi}{2}$, $D_{\omega P} > 0$ and $D_{\omega P}$ were proportional to $|G_{\omega P}(j\omega)|$. Therefore, to enable the active power ΔP_g of the DFIG-based wind farms to offer positive damping on SSR, the phase angle range of active-speed transfer function $G_{\omega P}(s)$ in the subsynchronous frequency band (62.8–314 rad/s) should be satisfied as follows:

$$\frac{\pi}{2} < \angle G_{\omega P}(j\omega) < \frac{3\pi}{2} \tag{12}$$

Design of SSR auxiliary damping controller

Structure of the SSR auxiliary damping control

The diagram of the auxiliary damping control system is shown in Fig. 4. SSR damping is achieved by addition of a supplementary signal at the active power loop of the RSC. Turbine generator speed $\Delta\omega$ served as the input signal; after processing by time delay, filter, and phase shift, a supplementary signal output of dynamic active power ΔP_g was provided and added at the active power loop of RSC.

where P_g and Q_g are the measured values of active/reactive power from the output ends of wind farms; P_g^*, Q_g^* are the set values of the active/reactive power of the converters, respectively; i_{dr}, i_{qr} are the rotor current values of shaft d and shaft q; i_{ds}, i_{qs} are the stator current values of shaft d and shaft q; u_{dr}, u_{qr} are the rotor voltages of shaft d and shaft q; l_r, l_m are the rotor self-inductance and stator mutual inductance; and ω_s is the slip angular frequency.

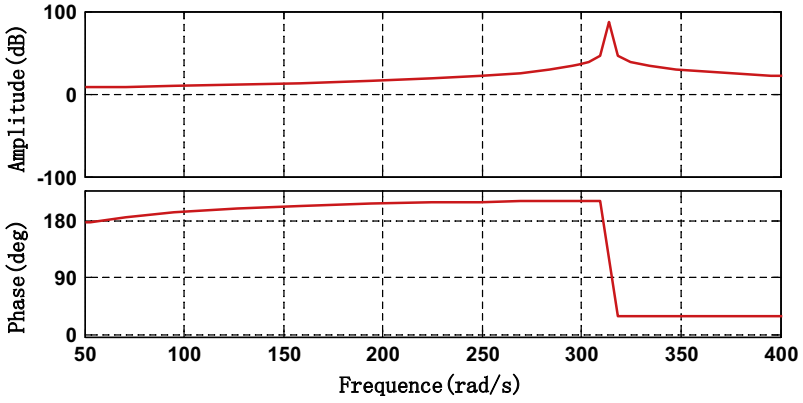

(a) Amplitude phase-frequency characteristic curve.

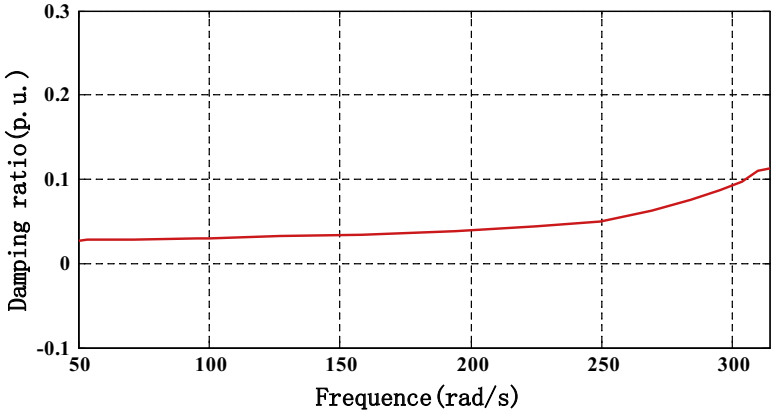

(b) Damping ratio curve.

Fig. 8. Characteristics of the transfer function with auxiliary damping control.

For an improved approximate time delay effect in the entire subsynchronous frequency band, we use Pade approximation for the time delay.

$$P(s)=\frac{\sum_{i=0}^{m}\frac{(m+n-i)!\,m!\,(-s\tau)^i}{i!(m-i)!}}{\sum_{i=0}^{n}\frac{(m+n-i)!\,n!\,(-s\tau)^i}{i!(n-i)!}} \tag{13}$$

where m, $n = 2$.

After time delay processing, the signal of turbine generator speed deviation $\Delta\omega$ was processed by the Butterworth filter to obtain the SSR modal component.

To efficiently compensate for the phase in the entire subsynchronous frequency band to satisfy the phase-frequency characteristics of damping SSR from Eq. (12), the proposed transfer function of the PID phase shift compensation is as follows:

$$G_C(s)=K_P\left(1+\frac{T_I}{s}+T_D s\right) \tag{14}$$

where K_P is the amplification gain, T_I is the integral time constant, and T_D is the derivative time constant. With SSR frequency ω_i, we let the phase compensation angle be $\phi_i=\angle G_C(j\omega_i)$, and $\tan\phi_i=T_D\omega_i-\frac{1}{T_I}\omega_i$. With proper controller parameters, the phases in the entire subsynchronous frequency band that can meet Eq. (12) can provide effective positive damping.

Optimization of the PID phase compensation parameters

To ensure that auxiliary damping controllers can provide effective positive damping in subsynchronous frequency bands, the proper phase compensation angle must be selected. Before calculating the phase compensation angle range, we must first determine the initial damping ratio and the initial phase angle range without auxiliary damping control. The amplitude-frequency and phase-frequency characteristic curve and the damping ratio curve were obtained, as shown in Fig. 5.

Next, based on the condition of the phase compensation angle range for positive damping from Eq. (12), the optimal parameters for PID phase control can be obtained. These parameters enable the controller to obtain effective damping controls in the entire subsynchronous frequency band. In our study, the goal was to

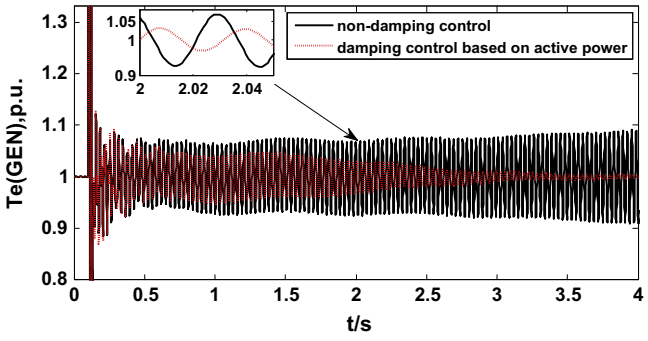

(a) Electromagnetic torque response of the turbine generator.

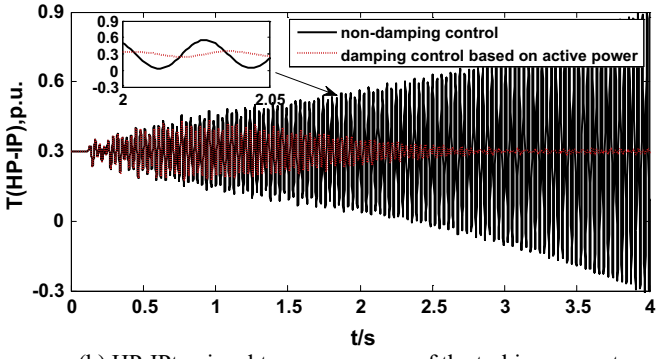

(b) HP-IPtorsional torque response of the turbine generator.

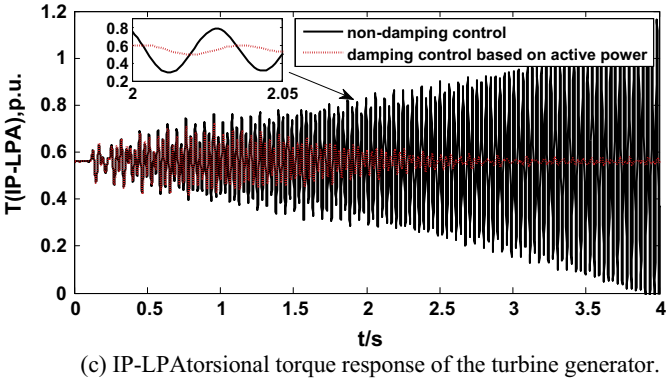

(c) IP-LPAtorsional torque response of the turbine generator.

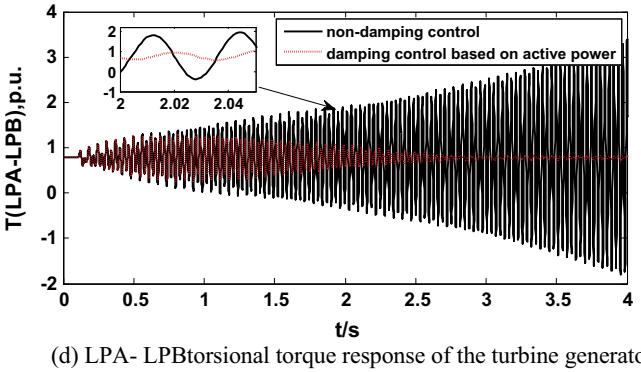

(d) LPA- LPBtorsional torque response of the turbine generator.

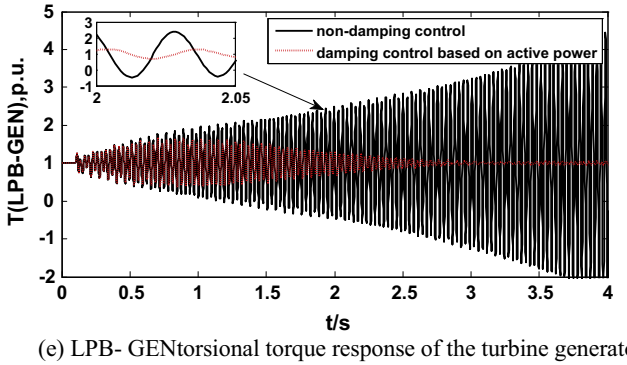

(e) LPB- GENtorsional torque response of the turbine generator.

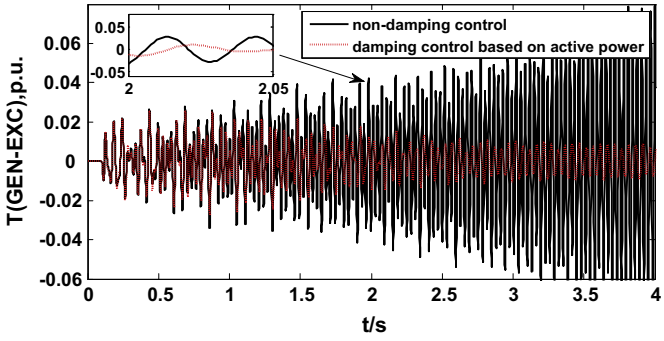

(f) GEN-EXCtorsional torque response of the turbine generator.

Fig. 9. Dynamic performance of the turbine generator during and after clearing fault.

make the eigenvalue of the closed-loop system approach the left of the complex plane as much as possible. The objective function is

$$T = \min_{\Phi_1}\{\max_{\Phi_2}\mathrm{Re}(\lambda)\} \quad (15)$$

where Φ_1 is the set of parameters of the PID controller (K_P, T_I, T_D); Φ_2 is the set of compensation level, which means the proportion of the series capacitive reactance to the line reactance (X_C/X_L); and $\max_{\Phi_2}\mathrm{Re}(\lambda)$ means to search the eigenvalue with maximum real parts (at given PID parameters) when the power system run at different compensation level Φ_2. $\min_{\Phi_1}\{\max_{\Phi_2}\mathrm{Re}(\lambda)\}$ means to search optimum PID parameters to make the minimum value of $\max_{\Phi_2}\mathrm{Re}(\lambda)$, in order to make the eigenvalue of the closed-loop system approach the left of the complex plane as much as possible.

The calculation process optimized by genetic algorithm is shown in Fig. 6.

In the figure, N_1 is the total number of iterations in the optimization. The value range of PID parameters and compensation level are set as: $K_P \in (0.1, 10)$, $T_I \in (1, 100)$, $T_D \in (1, 100)$, $X_C/X_L \in (0.2, 0.8)$. According to the above calculation process for the optimization of the phase compensation parameters of the PID controller, the changes in best fitness and mean fitness are shown in Fig. 7.

Table 1 shows the optimization of the phase compensation parameters of the PID controller.

Based on the optimization parameters of the PID controller, the amplitude-frequency and phase-frequency characteristic curve and the damping ratio curve of active-speed $G_{\omega P}(s)$ with the auxiliary damping control strategy were obtained, as shown in Fig. 8.

Comparison of Figs. 5 and 8 indicates that after the introduction of auxiliary damping control strategy based on the active power loop, the phase angle range of active-speed $G_{\omega P}(s)$ changed from $\pi/3$–$\pi/2$ to $\pi/2$–$3\pi/2$, which demonstrates that the damping effects changed from negative to positive and provided positive damping in the entire subsynchronous frequency band. Furthermore, the damping ratio curve shows that the damping ratio changed from negative to positive, and the damping ratio significantly increased compared with that without auxiliary damping control. This result is consistent with the findings on amplitude-frequency and phase-frequency characteristics.

Time domain simulation results

To evaluate the effectiveness of the proposed auxiliary damping control to mitigate SSR, the IEEE first benchmark model, modified by the inclusion of DFIG-based wind farms, was simulated with the use of the simulation program DigSILENT/PowerFactory. The compensation level X_C/X_L is to 0.55. At $t = 0.1$ s, a three-phase short-circuit fault occurred at bus A and lasted for 0.025 s. The time responses of the turbine generator torques and the angular acceleration during and after clearing fault with and without auxiliary damping control are shown in Fig. 9. Fig. 10 shows the DFIG electrical torque and the supplementary signal output of dynamic active power ΔP_g added at the active power loop of RSC.

Fig. 9 shows that when the auxiliary damping control of DFIG is not in service, the turbine generator shaft electrical torque, torsional torque, and angular acceleration exhibit severe torsional amplifications (instability) after clearing fault. When the auxiliary damping control of DFIG is in service, the turbine generator shaft

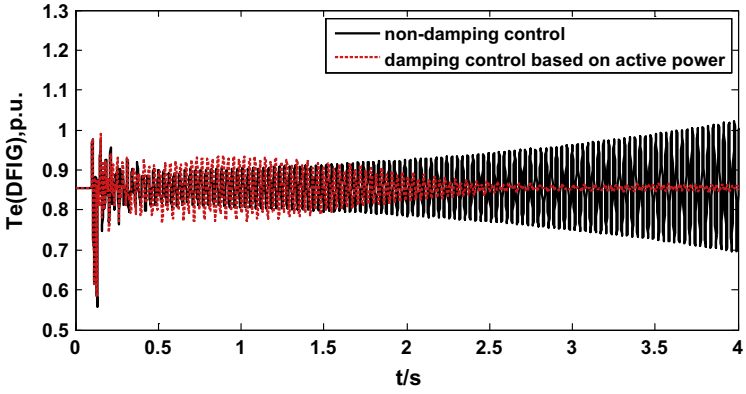

(a) Electromagnetic torque response of the wind turbines.

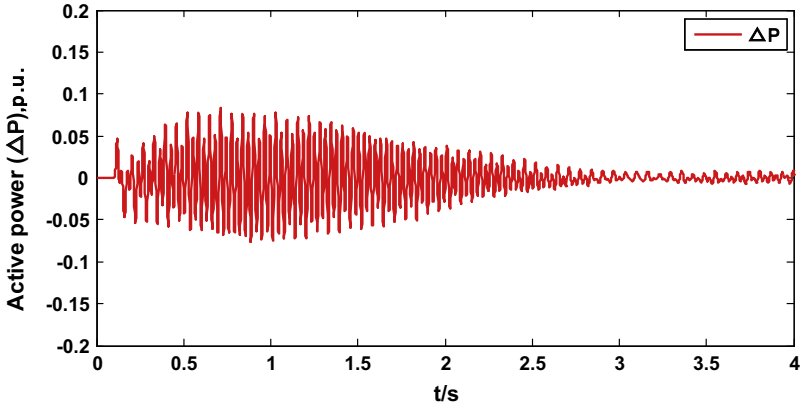

(b) Supplementary signal output of dynamic active power ΔP added at the active power loop of RSC.

Fig. 10. Dynamic performance of the wind turbine generator during and after clearing fault.

electrical torque, torsional torque, and angular acceleration are stable. These results demonstrate the effectiveness of the proposed auxiliary damping control in damping the SSR. Fig. 10(a) also shows that the adverse effect of SSR is extended to DFIG when the auxiliary damping control of DFIG is not in service, and the DFIG electrical torques also exhibit severe torsional amplifications (instability). When the auxiliary damping control of DFIG is in service, a supplementary signal output of dynamic active power ΔP is added at the active power loop of RSC, as shown in Fig. 10(b). The DFIG electrical torque is stable.

Conclusion

A novel auxiliary damping control strategy to mitigate SSR with the use of the active power control of DFIG-based wind farms has been presented in this study. Modulating the active power of the rotor-side converter of the DFIG to provide a positive damping component to facilitates SSR damping.

A transfer function between turbine generator speed and the output active power of wind farms was introduced to derive the analytical expression of the damping ratio. The effect of the active power of the DFIG-based wind farms on SSR damping was analyzed, and the phase range to obtain positive damping was determined. Then, a new auxiliary damping control strategy was proposed. The PID phase compensation parameters of the auxiliary damping controller were optimized by genetic algorithm to obtain the optimum damping in the entire subsynchronous frequency band. Finally, the effectiveness of the proposed auxiliary damping control in suppressing SSR oscillations is demonstrated through time domain simulation of the modified IEEE first benchmark model. Results show that the proposed auxiliary damping control can effectively damp SSR oscillations.

Acknowledgements

This study was supported by the National Natural Science Foundation of China (51377184), the International Science and Technology Cooperation Program of China (2013DFG61520), the Fundamental Research Funds for the Central Universities (CDJZR12150074), and the integration and demonstration program of Chongqing (CSTC2013JCSF70003). The authors are grateful for the support.

Appendix A

Network parameters

R_L = 0.02 pu, X_T = 0.14 pu, transformer ratio 26/539 kV, X_L = 0.50 pu, X_{sys} = 0.06 pu.

Turbine generator parameters

$X_{a\sigma} = 0.13$ pu, $X_d = 1.79$ pu, $X'_d = 0.169$ pu, $X''_d = 0.135$ pu, $X_q = 1.71$ pu, $X'_q = 0.228$ pu, $X''_q = 0.2$ pu, $T'_{d0} = 4.3$ s, $T''_{d0} = 0.032$ s, $T'_{q0} = 0.85$ s, $T''_{q0} = 0.05$ s.

Shaft parameters

H_{HP} = 0.092897, H_{IP} = 0.155589, H_{LPA} = 0.858670, H_{LPB} = 0.884215, H_{GEN} = 0.868495, H_{EXC} = 0.0342165, $K_{HP\text{-}IP}$ = 19.303 pu/rad, $K_{IP\text{-}LPA}$ = 34.929 pu/rad, $K_{LPA\text{-}LPB}$ = 52.038 pu/rad, $K_{LPB\text{-}GEN}$ = 70.858 pu/rad, $K_{GEN\text{-}EXC}$ = 2.82 pu/rad.

DFIG parameters

Rated power: 2 MW, rated voltage: 690 V, rated frequency: 60 Hz, wind speed: 11 m/s, R_s = 0.00832 pu, L_{ls} = 0.218 pu, R_r = 0.00935 pu, L_{lr} = 0.236 pu, L_m = 2.905 pu, H_g = 0.5 s, H_w = 4.45 s, K_s = 0.31 pu/rad.

References

[1] Maciej O, Balcerek P, Orkisz M. Effective method of subsynchronous resonance detection and its limitations. Electr Power Energy Syst 2012;43:915–20.
[2] Khazaie Javad, Mokhtari Maghsood, Khalilyan Mansour, Nazarpour Daryoush. Sub-synchronous resonance damping using distributed static series compensator (DSSC) enhanced with fuzzy logic controller. Electr Power Energy Syst 2012;43:80–9.
[3] Widyan Mohammad S. On the effect of AVR gain on bifurcations of subsynchronous resonance in power systems. Electr Power Energy Syst 2010;32(6):60–76.
[4] Bongiorno M, Svensson J, Angquist L. On control of static synchronous series compensator for SSR mitigation. IEEE Trans Power Electron 2008;23(2):735–43.
[5] Ghorbani A, Pourmohammad S. A novel excitation controller to damp subsynchronous oscillations. Electr Power Energy Syst 2011;33(3):411–9.
[6] El-Moursi Mohamed S, Bak-Jensen Birgitte, Abdel-Rahman Mansour H. Novel STATCOM controller for mitigating SSR and damping power system oscillations in a series compensated wind park. IEEE Trans Power Electron 2010;25(2):429–41.
[7] Jusan Fernando Cattan, Gomes Jr Sergio, Taranto Glauco Nery. SSR results obtained with a dynamic phasor model of SVC using modal analysis. Electr Power Energy Syst 2010;32:571–82.
[8] Bongiorno Massimo, Ängquist Lennart, Svensson Jan. A novel control strategy for subsynchronous resonance mitigation using SSSC. IEEE Trans Power Del 2008;23(2):1033–41.
[9] Farahani M. Damping of subsynchronous oscillations in power system using static synchronous series compensator. IET Gener Transm Distrib 2012;6(6):539–44.
[10] Varma RK, Auddy S, Semsedini Y. Mitigation of subsynchronous resonance in a series-compensated wind farm using FACTS controllers. IEEE Trans Power Del 2008;23(3):1645–54.
[11] Alomari MM, Nandakumar MP, Zhu JG. Bifurcation control of subsynchronous resonance using TCSC. Commun Nonlinear Sci Numer Simulat 2011;16(5):2363–70.
[12] Sindhu Thampatty KC, Nandakumar MP, Cheriyan Elizabeth P. Adaptive RTRL based new controller for damping subsynchronous oscillations using TCSC. Eng Appl Artif Intell 2011;24(1):60–76.
[13] Knuppel T, Nielsen JN, Jensen KH, Dixon A, Ostergaard J. Power oscillation damping controller for wind power plant utilizing wind turbine inertia as energy storage. Detroit, MI, Jul: IEEE Power and Energy Society General Meeting; 2011. p. 24–8.
[14] Fan Lingling, Yin Haiping, Miao Zhixin. On active/reactive power modulation of DFIG-based wind generation for interarea oscillation damping. IEEE Trans Energy Convers 2011;26(2):513–21.
[15] Miao Zhixin, Fan Lingling, Osborn Dale, Yuvarajan Subbaraya. Control of DFIG-based wind generation to improve interarea oscillation damping. IEEE Trans Energy Convers 2009;24(2):415–22.
[16] Tsourakis Georgios, Nomikos Basil M, Vournas Costas D. Contribution of doubly fed wind generators to oscillation damping. IEEE Trans Energy Convers 2009;24(3):783–91.
[17] Sherif OF, Irfan U, Dipendra R, Jean M. Utilizing DFIG-based wind farms for damping subsynchronous resonance in nearby turbine-generators. IEEE Trans Power Syst 2012;1(2):1–8.
[18] Hansena Anca D, Sørensena Poul, Iovb Florin, Blaabjerg Frede. Centralised power control of wind farm with doubly fed induction generators. Renew Energy 2006;31:935–51.